Detection of Myocardial Capillary Orientation With Intravascular Iron-Oxide Nanoparticles in Spin-Echo MRI

Alexandre Vignaud,[1] Ignacio Rodriguez,[1] Daniel B. Ennis,[3] Ranil DeSilva,[2] Peter Kellman,[1] Joni Taylor,[1] Eric Bennett,[1] and Han Wen[1]*

In mammalian hearts the capillaries are closely aligned with the muscle fibers. We report our observation of a main-field direction-dependent contrast in MR spin-echo (SE) images of the heart in the presence of Ferumoxtran-10, an intravascular iron-oxide nanoparticle contrast agent (CA). We describe a novel MRI method for mapping the preferential orientation of capillaries in the myocardial wall. The eigenvector corresponding to the minimum eigen value of the R_2 relaxation rate tensor is consistent with the expected orientation of the capillary network. Preliminary results also demonstrate the feasibility of this method for in vivo application to rodent imaging. Magn Reson Med 55:725–730, 2006. Published 2006 Wiley-Liss, Inc.†

Key words: magnetic susceptibility; cardiac MRI; USPIO; Ferumoxtran-10; T_2 tensor; capillary; myofiber; microvascular structure; diffusion; helical

The transmural helical structure of the myofibers in the heart and the consequent contraction pattern has been known for centuries (1–3), and so has the fact that the capillaries are closely aligned with the muscle fibers (3). We report our observations of a main magnetic field, B_0, direction-dependent contrast in MR spin-echo (SE) images of the heart in the presence of intravascular iron-oxide nanoparticles. The main external field direction dependence makes it possible to calculate the tensor components of the direction-dependent transverse relaxation rate (R_2 or $1/T_2$). The tertiary principal direction of the R_2 tensor coincides with the capillary orientation within the myocardial wall, and the correlation between the two can be explained by the physics of proton spin relaxation around the mostly parallel capillary vessels.

The nanoparticle contrast agent (CA) Ferumoxtran-10 is an aqueous solution that contains magnetite crystalline cores that are coated with dextran. They are too large to move across the pores of the endothelium of the capillaries and thus are confined to the intravascular space while they are slowly absorbed by the reticuloendothelial system of the liver. Because of their superparamagnetic nature they are fully magnetized in the field of a 1.5 Tesla MRI scanner (4), and create strong, heterogeneous, and localized fields around capillary vessels. In SE imaging, proton spins of tissue water undergo diffusive Brownian motion in these induced fields that accelerates T_2 relaxation. In the heart the capillaries are morphologically nearly parallel tubes that are aligned with the muscle fibers, and the field pattern around such a capillary is highly dependent on its orientation relative to the external main field (5), as illustrated in Fig. 1. The strongest local field gradients occur when the capillary is perpendicular to the main field, and as demonstrated by Monte-Carlo simulations of a capillary lattice in the heart (6), this condition should create the maximum T_2 relaxation and the lowest signal level in SE images.

We observed in both beating hearts and excised heart samples this variation of SE image intensity with orientation, as well as heterogeneous image intensity in the myocardial wall. We ruled out other potential instrumentation factors that might cause such heterogeneity with control images acquired using short echo times (TEs) and thus minimal T_2 relaxation. To characterize the directional dependence in the R_2 relaxation rate, we derived the second-order R_2 tensor from a set of images of an excised heart sample. A map of the tertiary eigenvector of the tensor, indicating the direction of minimum R_2, was then plotted throughout the myocardial wall. The results can be fully explained by the anisotropic R_2 relaxation in the presence of largely parallel capillaries, in the light of the well-known transmural helical patterns of the myofiber and capillary orientation of the heart (2) (i.e., the direction of minimum R_2 relaxation coincides with the myofiber orientation in all locations of the heart).

This observation provides a robust means of mapping the capillary orientation in vivo with simple SE imaging, and reducing susceptibility to physiological motion due to the lack of large motion-encoding gradients.

MATERIALS AND METHODS

Animal Preparation

The animal protocol was approved by the Animal Care and Use Committee of the National Institutes of Health and conformed to all relevant institutional and federal guidelines. For in vivo experiments, one beagle canine and one Sprague-Dawley rat were imaged. SE images were acquired before and after a slow intravenous injection of the superparamagnetic CA (4) Combidex (Ferumoxtran-10; Advanced Magnetics Inc, Cambridge, MA, USA) at a dose

[1]Laboratory of Cardiac Energetics, Division of Intramural Research, National Heart Lung and Blood Institute, National Institutes of Health, Bethesda, Maryland, USA.

[2]Cardiovascular Branch, Division of Intramural Research, National Heart Lung and Blood Institute, National Institutes of Health, Bethesda, Maryland, USA.

[3]Department of Radiology, Stanford University, Palo Alto, California, USA.

*Correspondence to: Dr. Han Wen, Imaging Physics Section, Laboratory of Cardiac Energetics, National Heart Lung and Blood Institute, National Institutes of Health, Bldg. 10, Room B1D416 MSC 1061, Bethesda, MD 20892-1061. E-mail: wenh@nhlbi.nih.gov

Received 19 May 2005; revised 2 December 2005; accepted 3 December 2005.

DOI 10.1002/mrm.20827

Published online 27 February 2006 in Wiley InterScience (www.interscience.wiley.com).

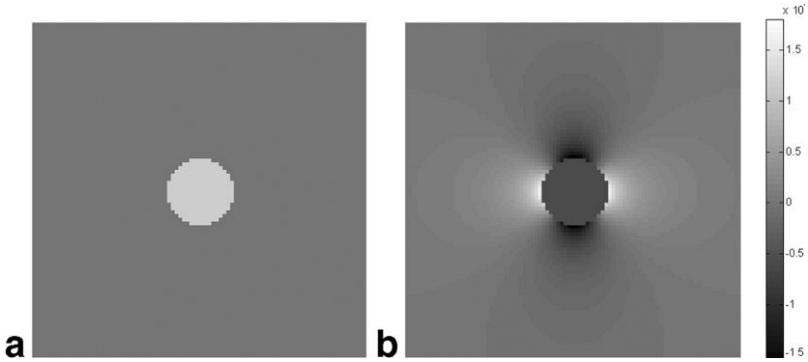

FIG. 1. **a:** Induced field ΔB around an infinite cylindrical vessel when B_0 is parallel to the vessel (5). **b:** Induced field corresponding to an orientation of B_0 perpendicular to the vessel. The model parameters are: vessel radius = 5.6 μm (9), magnetic susceptibility inside the vessel $\chi_i = 14.2 \times 10^{-6}$ with [Fe] = 15 mg/kg of body weight calculated for a total blood volume fraction of 8% (15), χ_m of Feromoxtran-10 (AMI 27) = 4.27 mol^{-1} cm^{-3} (16), and magnetic susceptibility of the surrounding tissue $\chi_e = -9.0 \times 10^{-6}$.

of [Fe] = 10 mg/kg and 30 mg/kg of body weight for the canine and rat, respectively. The canine was positioned along the main field of the scanner as allowed by the diameter of the scanner bore. The rat was small enough to be positioned both along and perpendicular to the main field.

To demonstrate how the image contrast changes with different orientations of the main field, the canine heart was excised immediately after euthanasia and embedded in a bottle of agarose gel. Before euthanasia was performed the [Fe] concentration was brought to 15 mg/kg of body weight. It was essential for the nanoparticles to remain in the blood vessels and prevent clotting during this process. Accordingly, the canine was heparinized and then euthanized by a bolus of KCl injected through the chest wall directly into the right ventricle. Then all of the arteries and veins that were directly connected to the heart were ligated with surgical suture lines, and the heart (still full of blood) was excised.

MRI Protocol

All scans were performed on a standard clinical 1.5 T scanner (Sonata; Siemens Medical Systems, Erlangen, Germany). The body coil was used for RF transmission. For the canine experiment a Siemens regular head coil was used for reception. The in vivo canine SE images of a single midventricular slice were acquired using the following parameters: TE = 8.0, 25.0, or 40.0 ms; image matrix dimensions = 256 × 112 × 1; voxel volume = 1.5 × 1.5 × 5.0 mm^3; receiver bandwidth = 256 kHz; and two averages. The acquisitions were performed during end-systole and in the relatively stationary end-expiratory plateau. The slice-selection and readout gradients were flow-compensated and both dark-blood and fat-saturation preparations were used. The dark-blood preparation was of the double-inversion type and included a volumetric π pulse followed by a slice-selective π pulse (7). The inversion time (TI) between the dark-blood preparation and SE acquisition was approximately 600 ms. A spectrally selective RF pulse was used for fat saturation immediately before acquisition. Much higher spatial resolution was required for the rat heart, and the following parameters were prescribed for the 3D SE scan: TE = 11.0 ms, image matrix = 256 × 112 × 10, voxel volume = 0.3 × 0.3 × 2.0 mm^3, receiver bandwidth = 90 kHz, and four averages. Two surface coils placed anterior and posterior to the chest of the rat were used for signal reception. The rat was scanned in two perpendicular orientations to observe the directional dependence of R_2 contrast in vivo.

To minimize water diffusion-related effects, the readout prephasing and phase-encoding gradients were placed immediately before readout. Gradient crushers along the

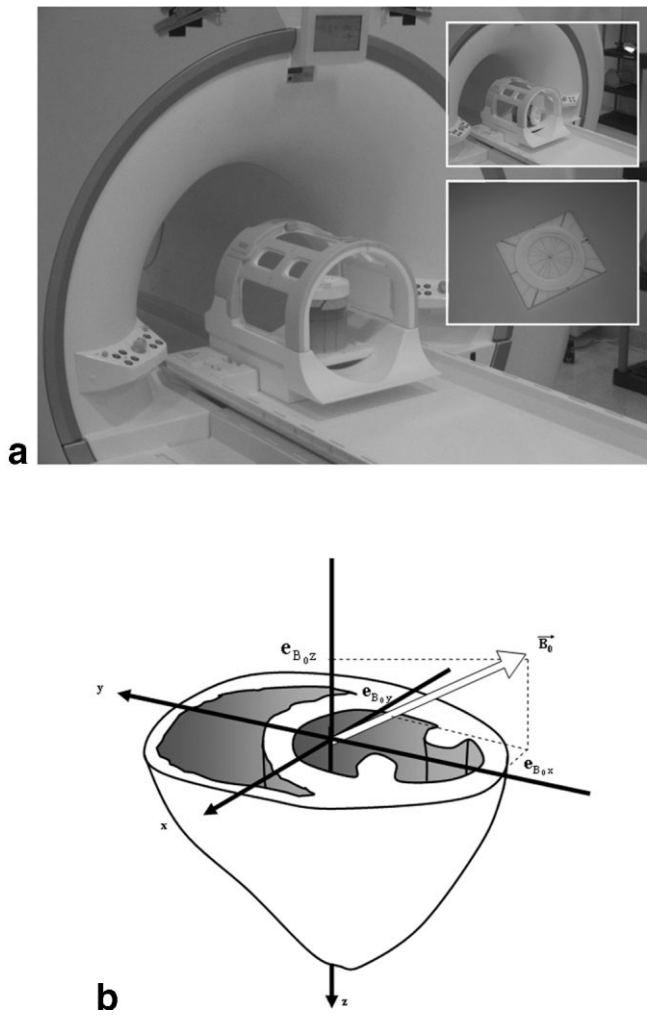

FIG. 2. **a:** Pictures showing the experimental setup. The top-right picture shows the heart specimen bottle in a vertical position. The bottom-right picture shows a closer view of the platform on which the sample bottle stands. The long axis of the heart was along the long axis of the bottle. **b:** Definition of the unit direction of $\vec{B}_0$, $\vec{e}_{B_0}$, relative to plane of the considered slice.

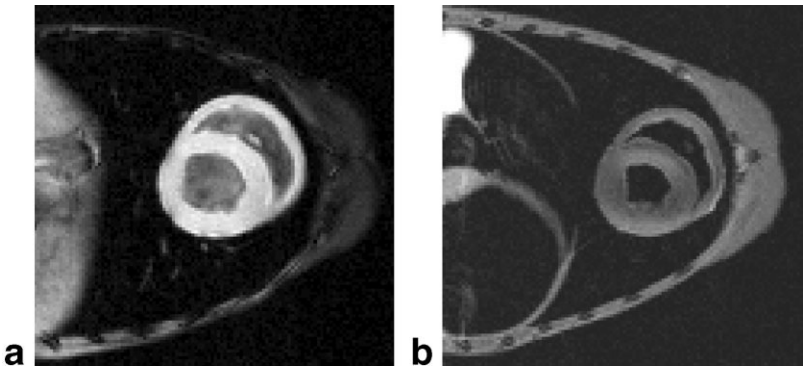

FIG. 3. Effect of the superparamagnetic CA on SE images. In vivo SE acquisitions in a canine heart (**a**) without and (**b**) with intravascular superparamagnetic CA ([Fe] = 10 mg/kg of body weight). Images were acquired with the same parameters (TE = 25 ms) except that for the acquisition without CA, dark-blood preparation and fat saturation were used.

slice-selection axis were placed on both sides of the π pulse, which had a diffusion weighting of $b = 14.2 \times 10^4$ s/m^2. The resulting signal attenuation was a negligible 0.02 % in the myocardium.

The single midventricular slice of the excised canine heart was scanned in seven different noncollinear directions using the same imaging parameters used for the in vivo scans, except that the slice-selection gradients were not flow-compensated and no dark-blood or fat-saturation pulses were needed. Reference images of a fixed orientation were acquired between each change of orientation to assess the degradation of the heart over the time of the experiments. To obtain accurate orientations of the bottle, it was marked with a compass and placed on a custom-made stage with angle markers. The stage was designed to align the center of the bottle with the isocenter of the magnet. The different orientations were accomplished by rotating the bottle on its side or base using the markers as references (Fig. 2a). The slice position was then determined with gradient-echo (GRE) scout images of the horizontal and vertical markers placed all around the bottle. Images were registered (8) before a R_2 tensor map was created by fitting the logarithm of the image intensity of each pixel to an ellipsoid in the space of main field orientation:

$$I(e_{B_0}) = I_0 e^{-e_{B_0}^T R_{2,T} e_{B_0} TE} \quad [1]$$

where I is the intensity of the signal as a function of the main field orientation e_{B_0} (Fig. 2b), I_0 is the signal intensity immediately after the radiofrequency (RF) excitation, $\boldsymbol{R_{2,T}}$

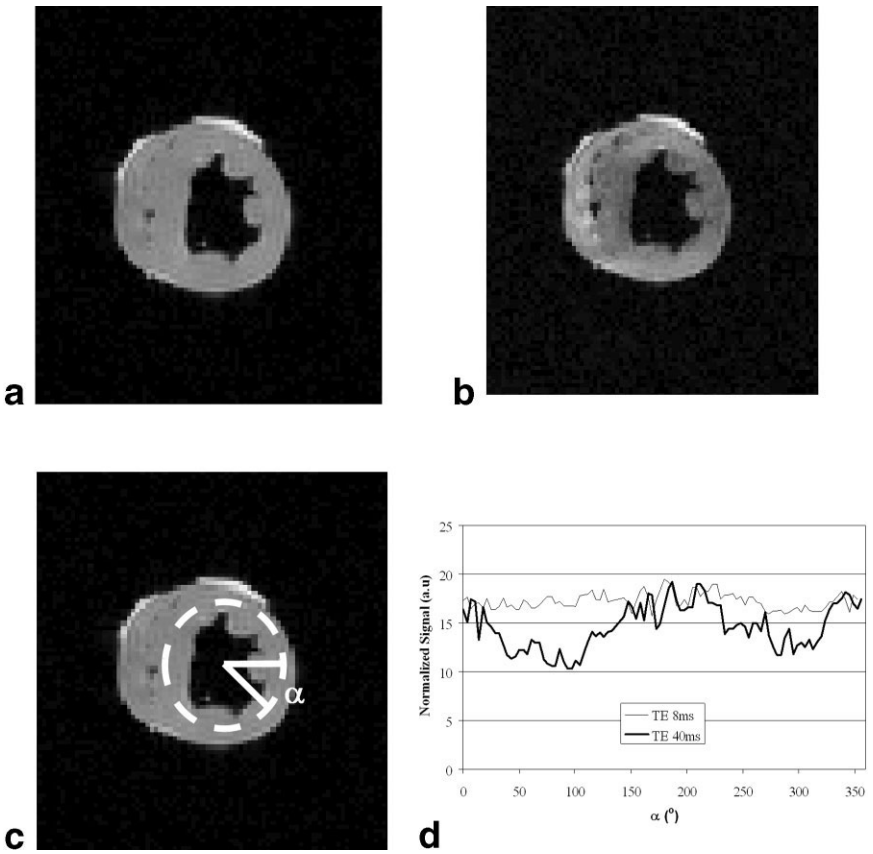

FIG. 4. Demonstration of the R_2 effect of the superparamagnetic CA. **a:** SE (TE = 8.0 ms) midventricular short-axis image ex vivo without blood in the ventricles with 15 mg/kg of body weight of CA. **b:** The same SE scan with TE = 40.0 ms. **c:** Circumferential path in the mid-layer of the LV wall along which the image intensity was measured for both a and b. **d:** Evolution of the normalized image intensity along the circumferential path.

is the tensor form of the relaxation rate R_2, and TE is the echo time of the SE sequence. The axes of the ellipsoid are then the eigenvectors of the R_2 tensor. The main direction of the capillary vessel corresponds to the third eigenvector, which is the direction of minimal R_2.

RESULTS

Main-Field Direction-Dependent Image Contrast in Beating Hearts

The two SE images displayed in Fig. 3 were acquired from the canine in vivo, respectively without and with the superparamagnetic CA. Whereas the image intensity prior to contrast injection was uniform, a nonuniform pattern in the walls of the heart was caused by the CA.

To identify the cause of this nonuniformity, we acquired images with a short TE (8.0 ms). The results did not show the spatial heterogeneity in signal intensity or the dependence on orientation of the main field, as illustrated in Fig. 4a and b. Therefore, instrumental factors that might have caused image intensity variation, such as nonuniform RF excitation field or signal reception were not the source of the intensity pattern. Additionally, the large amount of CA in the blood pool of the ventricular cavities creates susceptibility fields that extend into the myocardial wall. This remote field affects T_2*-weighted images but not SE images. To confirm this point, we observed the signal pattern in the myocardial wall after removing the blood (Fig. 4). Once these factors were ruled out, the cause of the signal pattern was recognized as a change in the myocardial R_2 brought about by the CA.

R_2 Tensor Mapping in the Heart Specimen

The excised heart specimen was imaged with a set of seven different orientations of B_0 relatively to the selected slice. The reference images were acquired before each scan in the same orientation, and did not show significant variation of signal over the duration of the experiment (approximately 2 hr) that could result from degradation of the fresh heart tissue (Fig. 5a). Figure 5b demonstrates how the pattern of intensity variation in the myocardium depends on the direction of B_0. Using this set of data, we quantified the local capillary orientation by measuring the angle between the tertiary eigenvector of the R_2 tensor and the local circumferential plane, as illustrated in Fig. 6. To define this angle, we defined a local cardiac coordinate system defining the radial, circumferential, and longitudinal directions from the geometry of the left ventricle. The circumferential direction points counterclockwise when the image is viewed from the apex to the base. Because the result of the eigenvector calculation is a vector that can point along either of two antiparallel directions, the tertiary eigenvector was defined as the vector closest to the aforementioned circumferential vector. The orientation angle was calculated as the angle between the tertiary eigenvector and the circumferential direction. The sign of the angle is positive if the eigenvector points toward the base, and negative if it points toward the apex. The direction of minimum R_2 has the following features: the orientation in the imaging plane generally courses along the circumference of the ventricular walls; in the left ventricular wall the vectors generally start at nearly vertical angles relative to the epicardial layer, and rotate continuously toward the imaging plane, cross the plane in the mid layer of the ventricular wall, and continue to rotate away from the plane until they are almost vertical again at the endocardial surface; and the vectors are generally perpendicular to the imaging plane in the papillary muscles. It was previously shown that, similarly to humans, canines have a network of capillaries that parallel the myofibers (9). These features are similar to the myofiber orientations in the heart, which have been established by anatomical dissection (2) and diffusion tensor imaging (DTI) in various mammals (10–12).

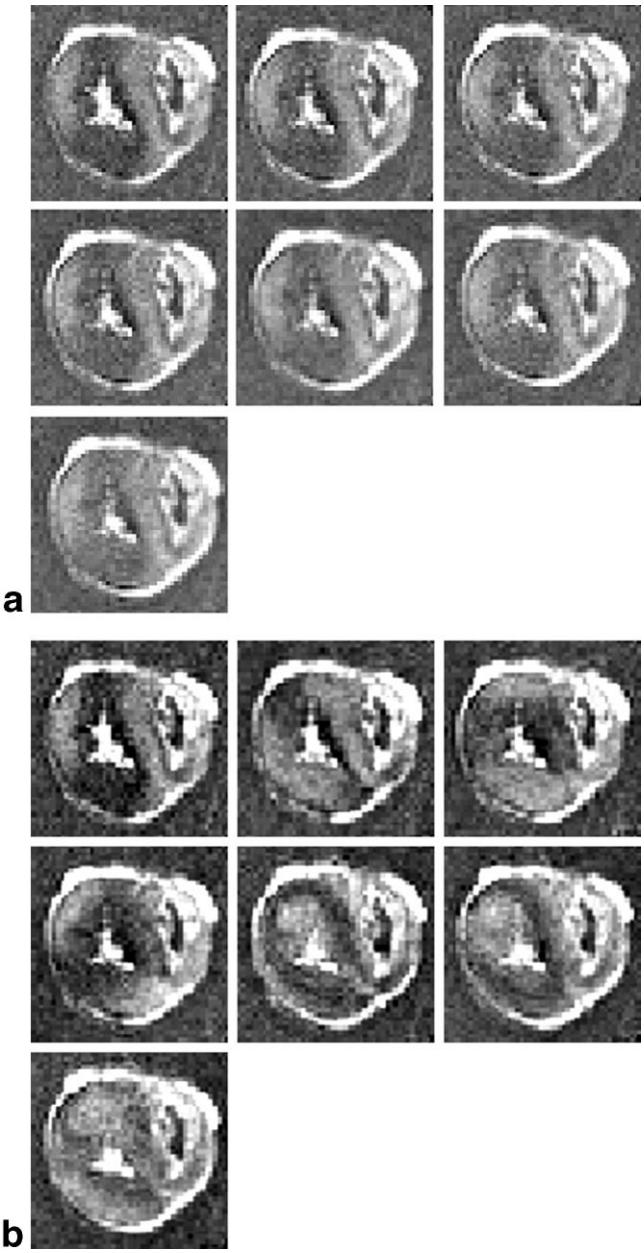

FIG. 5. **a:** Reference images acquired for e_{B_0} [–1 0 0] relative to the selected slice in 10–15-min intervals. **b:** Images acquired for the different B_0 orientations relative to the slice (from top left to bottom right): e_{B_0} = [–1 0 0], [–1 –1 0], [0 –1 0], [1 –1 0], [0 0 1], [–1 0 1], [0 1 1].

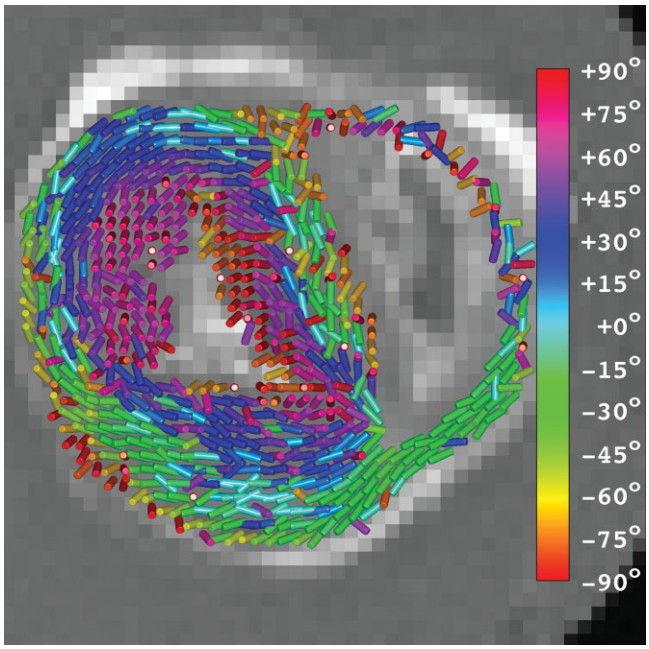

FIG. 6. 3D representation of the tertiary eigenvector of the R_2 tensor map superimposed on an image of the short-axis slice. The R_2 tensor map was computed from data for seven directions of B_0. The color code indicates the angular deviation from the imaging plane, and 90° is orthogonal to the image plane. The background image is the image of orientation e_{B_0} [–1 0 0] (Fig. 5b).

DISCUSSION

There is clear evidence that the heterogeneous signal intensity in SE images of the heart in the presence of a superparamagnetic CA is due to the anisotropic T_2 relaxation from largely parallel capillaries in the myocardium. The tensor component of the R_2 relaxation coefficient also coincides with myofiber orientations. This observation provides a means of mapping capillary structure in vivo using SE MRI and an intravascular CA. The method requires the rotation of the main magnetic field relative to the heart and therefore is easier to realize in small animals, such as rodents. This was demonstrated in a rat in vivo, as illustrated in Fig. 7a and b. In pathological conditions in which the myofiber and the capillary structures are coupled (13,14), this method could eventually be used indirectly to detect myofiber organization. It could be especially useful for small animals, in which DTI is challenging.

The main technical challenge of this method is the rotation of the sample and registration of the images from different orientations. For example, the images in Fig. 7 were acquired by simply rotating the animal 90° between the two surface coils to the best of our judgment, and the result was an apparent difference in signal intensity pattern between the two images. For a more systematic approach, a custom-built rotation stage that allows planar and axial rotation around the isocenter of the magnet is needed. Once the bulk orientation is controlled accurately, the position and orientation of the heart may still shift within the chest cavity. Fortunately, in small animals the weight of the heart itself is low, and any shift of the heart in the chest can probably be corrected with the use of image registration methods.

The profile of angle distribution obtained throughout the myocardial wall (Fig. 6) was not as smooth as those obtained using DTI (10). This likely reflects the fact that our SE scan is relatively short compared to classic ex vivo DTI scans, which results in a lower signal-to-noise ratio (SNR) and lower number of orientations acquired. It is reasonable to expect that there is an optimal setting of contrast concentration and TE to obtain the best contrast-to-noise ratio (CNR), and that this setting will depend on the main field strength and intrinsic relaxation times of the tissue involved.

CONCLUSIONS

The novel technique presented here is the first to use contrast-enhanced MRI to map the capillary network organization. This technique has the potential to reveal changes in capillary organization that may occur in microvascular disease, cardiomyopathy, and ventricular remodeling.

It is conceivable that at very high fields the susceptibility of deoxyhemoglobin itself is sufficient to create the R_2 tensor effect; however, this remains to be tested. Anisotropic capillary structures are also present in other organs, such as the brain, kidney, and skeletal muscle. The R_2 tensor phenomenon may therefore have applications outside the myocardium.

ACKNOWLEDGMENTS

The authors thank Paula Jacobs and Advanced Magnetics Inc. for providing the CA and the relevant safety data.

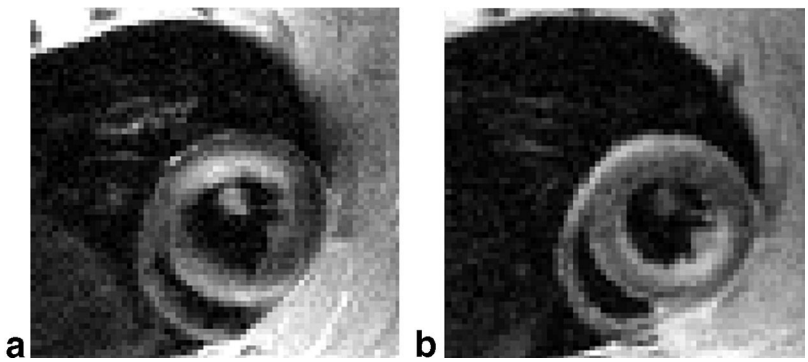

FIG. 7. Demonstration of the feasibility of the proposed method for rodent in vivo imaging. **a:** SE (TE = 11.0 ms) midventricle short-axis image in vivo in a rat with 30 mg/kg of body weight of superparamagnetic CA. The rat was laid along B_0. **b:** Same scan of approximately the same slice, but with the rat lying perpendicular to B_0. The patterns revealed in these images differ: in a the enhanced areas are in the endocardial layer of the anterior wall and the epicardial layer of the posterior wall, and in b the pattern is reversed.

They also thank Kathryn Hope, and Catherine Lucas for their help in caring for the animals.

REFERENCES

1. Harvey W. An anatomical disquisition on the motion of the heart and blood in animals (1628). In: Willis FA, Keys TE, editors. Cardiac classics. London: Henry Kimpton; 1941. p 19–79.
2. Streeter Jr DD, Spotnitz HM, Patel DP, Ross Jr J, Sonnenblick EH. Fiber orientation in the canine left ventricle during diastole and systole. Circ Res 1969;24:339–347.
3. Greenbaum RA, Yen Ho S, Gibson DG, Becker AE. Left ventricular fibre architecture in man. Br Heart J 1981;45:248–263.
4. Jung CW, Jacobs P. Physical and chemical properties of superparamagnetic iron oxide MR contrast agents: Ferumoxides, Ferumoxtran, Ferumoxsil. Magn Reson Imaging 1995;13:661–674.
5. Haacke EM, Brown RW, Thompson MT, Venkatesan R. Magnetic resonance imaging physical principles and sequence design. New York: Wiley-Liss; 1999. p 751–753.
6. Kennan RP, Zhong JH, Gore JC. Intravascular susceptibility contrast mechanisms in tissues. Magn Reson Med 1994;31:9–21.
7. Edelman RR, Chien D, Kim D. Fast selective black blood MR imaging. Radiology 1991;181:655–660.
8. Thevenaz P, Unser M. A pyramid approach to subpixel registration based on intensity. IEEE Trans Image Processing 1998;7:27–41.
9. Bassingthwaighte JB, Yipintsoi T, Harvey RB. Microvasculature of the dog left ventricular myocardium. Microvasc Res 1974;7:229–249.
10. Hsu EW, Muzikant AL, Matulevicius SA, Penland RC, Henriquez CS. Magnetic resonance myocardial fiber-orientation mapping with direct histological correlation. Am J Physiol 1998;274:H1627–H1634.
11. Scollan DF, Holmes A, Zhang J, Winslow RL. Reconstruction of cardiac ventricular geometry and fiber orientation using magnetic resonance imaging. Ann Biomed Eng 2000;28:934–944.
12. Tseng WYI, Wedeen VJ, Reese TG, Smith RN, Halpern EF. Diffusion tensor MRI of myocardial fibers and sheets: correspondence with visible cut-face texture. J Magn Reson Imaging 2003;17:31–42.
13. Tomanek RJ, Searls JC, Lachenbruch PA. Quantitative changes in the capillary bed during developing, peak, and stabilized cardiac hypertrophy in the spontaneous hypertensive rat. Circ Res 1982;51:295–304.
14. Oosthoek PW, Moorman AFM, Sauer U, Gittenberger de Groot AC. Capillary distribution in the ventricles of hearts with pulmonary atresia and intact ventricular septum. Circulation 1995;91:1790–1798.
15. Albert MS, Huang W, Lee J-H, Patlak CS, Springer CS. Susceptibility changes following bolus injections. Magn Reson Med 1993;29:700–708.
16. Weisskoff R, Kiihne S. MRI susceptometry: imaged-based measurement of absolute susceptibility of MR contrast agents and human blood. Magn Reson Med 1992;24:375–383.